Journal of Hydronautics

VOLUME 4 APRIL 1970 NUMBER 2

Design Aspects of Stern-Mounted Propellers for Deep-Submergence Vehicles

JOHN A. MERCIER*
Stevens Institute of Technology, Hoboken, N. J.

This paper presents the results of model tests carried out on two alternate hull configurations for a proposed deep-submersible vessel. The experiments consisted of resistance tests, propeller tests, self-propelled tests to derive the propeller-hull interaction effects for a range of vehicle drags (corresponding to different amounts of externally-mounted, resistance-increasing equipment), and Pitot-tube wake surveys carried out in way of the propeller plane. The two configurations differed in respect to the relative stubbiness of their afterbodies, both having a single relatively large diameter, stern-mounted propeller. The data are analyzed and comparisons are made with alternate propulsion configurations. The influence of propeller diameter on power and rpm is studied. A discussion of relevant data available in other sources is presented. A recommendation is made to carry out full-scale resistance tests of deep-submergence vehicles by the method of free deceleration.

I. Introduction

HULL shapes for many of the deep-submergence and submersible vehicles which are now being developed may reasonably be described as hydrodynamically peculiar. Many of these shapes differ significantly from rotationally symmetric, well streamlined forms because of functional requirements and design exigencies. Access tower locations, externally mounted equipment, viewing port, and maneuvering device arrangements seem to combine in many instances to give configurations which are apparently hydrodynamically "dirty," having high drag. Consideration of the profiles of some of the vehicles shown in Fig. 1 which were taken from a paper by Wenk,[1] should be sufficient to illustrate the point. These remarks are, of course, not equally applicable to all designs, some of which are carefully and effectively streamlines. They are also not intended to be in any way derogatory, it being appreciated that vehicle designers have cogent reasons for accepting less-than-optimum hull shapes.

Although design tradeoff may be dictated which prejudice the propulsive efficiency of some of these vehicles, it must be clearly evident that the penalties should be minimized. The relationship between the specified speed and endurance and the required propulsive power determines the size of propulsion unit and energy source, which, in turn, is an important factor in weight, displacement, payload, and size.

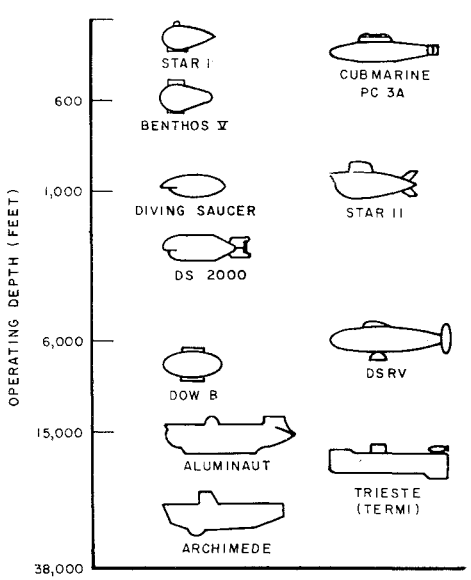

Fig. 1 Profiles of deep-submergence vehicles adapted from Ref. 1.

Presented as Paper 69-392 at the AIAA 2nd Advanced Marine Vehicles and Propulsion Meeting; submitted July 7, 1969. Work partly supported by Westinghouse Electric Corporation, Ordnance Division, Baltimore, Md. The author is grateful to Westinghouse Electric Corporation for permitting the results of tests conducted under their sponsorship to be presented and to the Director, Davidson Laboratory, for supporting additional analysis and preparation of this paper.

* Research Engineer, Davidson Laboratory.

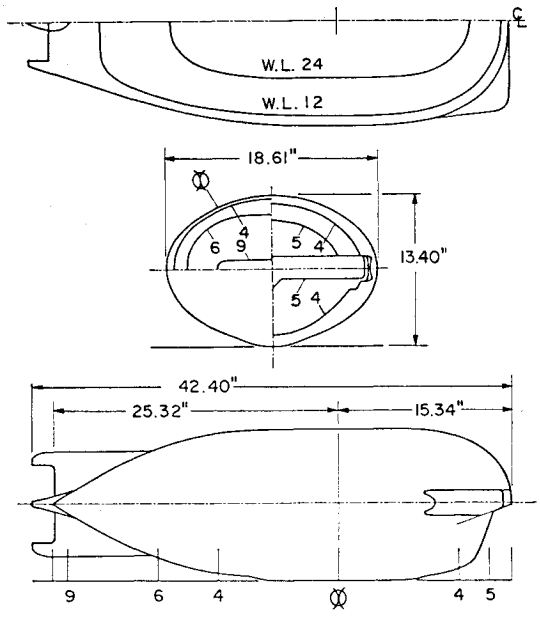

Fig. 2 Long afterbody model.

The resistance and propulsion qualities of unconventional submersible hull forms, which may have large appendages and substantial exterior-mounted equipment, are difficult to estimate. For some configurations, the lack of previously acquired experimental data for related forms makes the estimate of drag almost speculative. Some guidance, to be sure, can be found in published literature, especially in the very useful compilation by Hoerner,[2] which contains a wealth of information on resistance. The situation with respect to propulsion, especially propeller-hull interaction, is much less satisfactory.

The results of comprehensive model powering tests carried out with two alternate hull configurations for a proposed submersible vessel are presented in this paper. The experiments consisted of resistance tests, propeller tests, self-propelled tests to derive propeller-hull interaction effects for a range of vehicle drags (corresponding to different amounts of externally mounted, resistance-increasing equipment), and Pitot-tube surveys of the velocity distribution in the propeller plane. The two configurations differed only in the relative stubbiness of their afterbodies, both having a single relatively large diameter stern-mounted propeller.

The data are analyzed and comparisons made between the power requirements for one of these vehicles using a stern-mounted propeller and a similar hull fitted with wing-mounted propellers. The substantial power advantages associated with the propeller's operating in the wake region are indicated. It is shown that while a stubbier afterbody may result in greatly increased resistance, the power requirements may be only slightly different than for a finer afterbody. Using the results of the wake-survey test, the effect of propeller diameter on the power requirements and the optimum propeller rpm are investigated.

The presentation of the model test results is accompanied by discussion of and references to other pertinent published data and analysis procedures. It is hoped that the specific information given will be of interest and that, in conjunction with the discussion, it will also be useful.

Since virtually all scale model tests of vehicles must be conducted at lower Reynolds numbers than that at which the full-scale vehicle will operate, the possibility of scale effect on resistance and power exists. This is particularly true when a vehicle has extraneous unfaired appendages. Stubby afterbodies may also be prone to separation, and scale effect on this flow phenomena is not clearly understood. Powering standardization trials, in which speed, propeller rpm, torque, and thrust are evaluated, as for thorough surface ship standardization trials, should provide data useful for future design applications. A recommendation is made to carry out and report full-scale resistance tests of these deep-submergence vehicles by the method of free deceleration, which previously has been applied to airships and other vehicles.

II. Powering Tests

The powering experiments were carried out and evaluated according to procedures which are well established in the ship design field. Separate resistance and propeller characterization tests were conducted and self-propelled tests performed for a range of loadings with both of the models being fitted with each of two propellers. Results of these tests, and their analysis, as well as the results of the Pitot wake survey will be discussed in separate sections. This is convenient since the methods used in accounting for the net power requirement of the full-scale vehicle, and for providing information for propeller design, call for separate evaluations of all of these tests, not simply a scaling-up of the measured model power, although this may be done under specific conditions.

Outline drawings of the two models, which differ from one another only in the afterbody shape, are given above (Figs. 2 and 3). The models were fabricated of glass-reinforced epoxy, with $\frac{1}{16}$-in.-thick sheet aluminum for the vertical tail fins. The size of the model was selected in order to satisfy as nearly as possible three basic requirements: 1) the model should be small enough compared to the size of the test tank so that blockage effects are not significant, 2) the model should be large enough so that above-critical Reynolds numbers can be achieved, and 3) existing instrumentation and force balances should fit within the model skin. Propeller diameter was selected so that the propeller would fit, with adequate clearances, within the available aperture provided by the protective skegs and be sufficiently large to achieve good propulsive qualities. The models represent a prototype with a pressure hull diameter of 5 ft, corresponding to a scale ratio of 4.5.

Resistance Tests

A sketch illustrating the model, as set up for resistance testing, is given in Fig. 4. Tests were conducted in Davidson Laboratory's Tank No. 3, which is 300 ft long, 12 ft wide and 6 ft deep. The centerline of the model is submerged to a depth of about $30\frac{1}{2}$ in. The model is mounted so that the underbody of the vehicle faces the surface of the water be-

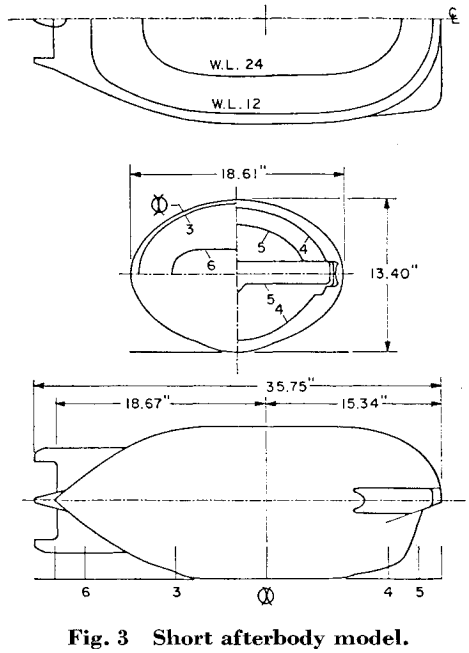

Fig. 3 Short afterbody model.

cause the installation of force measuring devices within the model was thereby facilitated. The model was rigidly connected to the carriage by a streamlined hollow strut. Electrical leads for instrumentation and power supply to the propeller drive motor, as well as tubing for inert gas for pressurizing the watertight propeller motor containment vessel, were carried through this hollow strut.

The resistance of each model was measured with a stiff-spring force balance mounted inside the model, connecting the model and strut. A range of speeds were tested in order to determine the influence of speed on the drag coefficient, C_D = (resistance)/(ρ/2) (speed)^2 (projected frontal area), where ρ is the fluid mass density. The projected frontal area for both the long and short afterbody models is 1.321 ft^2.

Results of the tests are presented in Fig. 5, where C_D is plotted against model speed with auxiliary scales of Reynolds number, R_n = (speed) (model length)/(kinematic viscosity) for both the long and short models. Tests were carried out with water temperature of 70.5°F, and the corresponding viscosity of water obtained from standard tables.[3] When making resistance tests on bodies for which extensive flow separation occurs and the preponderance of the measured drag is attributable to the defect in fluid pressure over the after part of the body due to the flow separation, it is found that there is a critical R_n below which the flow in the boundary layer is laminar and separation occurs relatively far forward on the model, giving rise to large pressure drag and unstable resistance. Above the critical R_n, the separation point moves aft and the drag decreases markedly. It may be noted that, according to Hoerner,[2] the transition from laminar to turbulent flow occurs at lower Reynolds numbers in water than in air; consequently, towing tank tests may be considered more suitable than wind-tunnel tests for this kind of experimentation.

When a model is towed in proximity to the water surface, waves may be generated which will give rise to additional resistance. The increase in drag at speeds above 4 fps for the long model and 3.5 fps for the short model, as shown in Fig. 5, is attributable to wavemaking. The nature of the resistance curves and the absence of data scatter at speeds below wavemaking speeds indicate that the flow is indeed above critical. Tests were limited to speeds below 8 fps by the capacity of the particular drag balance used. A theoretical estimate of wave drag may be obtained from results of calculations by Wigley[4] for submerged spheroids. For a speed of 6.5 fps, the wave drag coefficient of a spheroid equivalent to the long afterbody model may be derived from Wigley's tables as

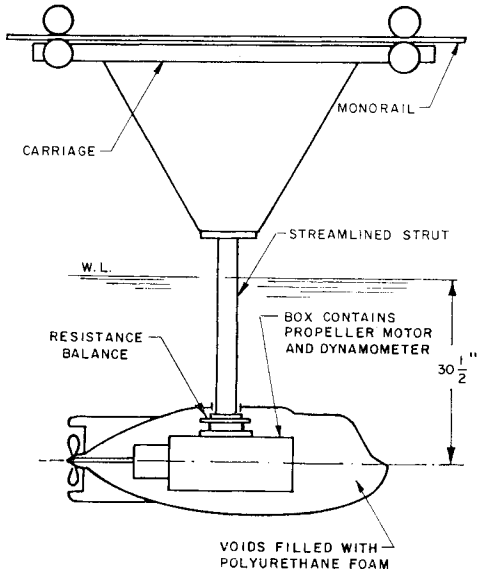

Fig. 4 Model test setup.

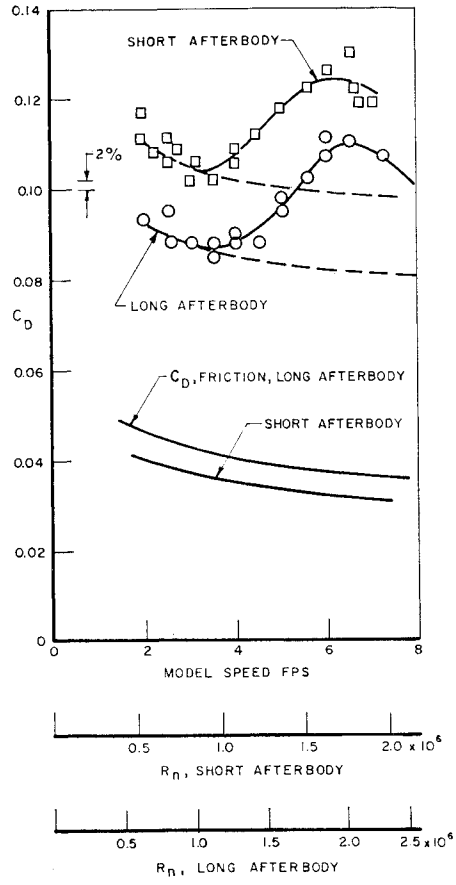

Fig. 5 Resistance test results.

$C_{DW} \approx 0.016$. This coefficient is defined in the same way as the drag coefficient of Fig. 5 except the theoretical wave resistance is used rather than the experimental total measured resistance. The observed wave drag is substantially greater than this theoretical value, as can be seen in Fig. 5. This is, in general, not unusual for correlation of theoretical wave resistance and experimental findings and, of course, the models in question differ greatly from the theoretical spheroids. The measured data cannot be adequately corrected for the effect of wave drag using this simplified theory and the results must be corrected according to the experimenters experience and judgment.

The dashed extrapolated lines shown in Fig. 5 represent the drag coefficient as a function of speed in the absence of wave generation. These curves were derived by assuming that the difference between the measured specific drag and the specific frictional resistance of an equivalent flat plate are the same at all speeds as they are at 3 fps. The equivalent flat plate is one whose length is equal to the model length and whose wetted surface is equal to the integral of the wetted girths of body stations of the models. The specific frictional resistance C_{Dfric} is obtained from Schoenherr's formulation, tabulated in Ref. 3, and accounts for less than half of the measured resistance for both models, as is shown in Fig. 5.

The assumption that the difference between measured specific drag and the specific frictional resistance of the equivalent plate is independent of the Reynolds number R_n was first used by Froude in 1874. This difference was referred to as residuary resistance which, in Froude's case, varied with the ratio of speed to the square root of length [a parameter which was later formalized to become the Froude No. $F_n = V/(gl)^{1/2}$] because wave generation effects were being accounted for. In the absence of wave generation, the residuary resistance is called "form effect" by Naval Architects and contains components of viscous shear due to the

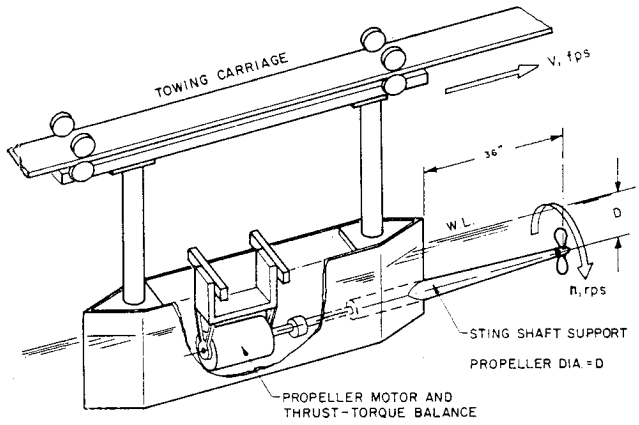

Fig. 6 Propeller test boat.

augment to fluid velocity along the sides of the full body and components of viscous pressure drag. This differs from the aerodynamicist's "form drag" which is intended to include only the pressure drag. The scale effects on the two kinds of viscous resistance are not clearly understood although for turbulent flow with a fairly stable separation region, all of the viscous shear drag would be expected to vary with R_n in a manner similar to that for flat-plate friction. Scale effect on viscous pressure drag, for above critical R_n cannot be described with great accuracy, even for simple shapes whose drag is primarily due to viscous pressure, such as spheres[2] and cylinders,[5] where all the test data are limited to values of R_n less than 10^7. There have been indications that this component of drag may increase with increasing R_n,[6] so that the assumption of constant specific residuary resistance may not be overly conservative.

It should be noted that the drag of the short afterbody model is about 20% higher than that of the longer model although the shorter model displaces significantly less volume.

Resistance Comparisons

The drag of the long afterbody model will be estimated according to two methods which are available in the published literature for application to streamlined bodies of revolution, and the estimates compared with the measured data. The equivalent diameter of the model, which has a maximum section area of A_M will be taken as $d_{eq} = (4A_M/\pi)^{1/2}$, or 15.56 in. for this model. The model length is shown in Fig. 2 to be 42.4 in.

Hoerner,[2] in Eq. (28), gives a formula for the drag of a body of revolution without appendages for turbulent flow, as

$$C_D/C_{D,\text{fric.}} = 1 + 1.5(d_{eq}/\text{length})^{3/2} + 7(d_{eq}/\text{length})^3 \quad (1)$$

The second term of Eq. (1) accounts for the augment to viscous friction while the third term is due to separation. $C_{D,\text{fric.}}$ may be estimated from the Schoenherr formulation as before. For d_{eq}/length of 0.367 the drag from Eq. (1) is found to be 1.68 times the equivalent flat plate friction. The drag of the fins must be accounted for separately, and Hoerner[2] indicates in the section on "Drag of Airships" in Chap. XIV that the additional drag due to fins is larger than corresponding to friction drag of their wetted area, the amount depending on the particular arrangement. The total wetted surface of the vertical fins is approximately 0.79 ft^2, the effective length about 10 in., and the corresponding $C_{D,\text{fric.}}$ is 0.0035, or almost 5% of the bare hull drag. No account has been taken of the finite hull trailing-edge breadth, which might be considered as a sort of fin, but a suitable way to define its effective area is difficult to conceive. The total drag, including the fin drag as computed according to its skin friction, since the fins are very thin, is $C_{D,\text{est.}} = 0.0774$ for a speed of 3 fps. This value is 11% lower than the measured $C_D = 0.0875$.

Table 1 Propeller characteristics

Propeller	A	B
Number of blades	3	3
Diameter D, ft	0.518	0.518
Pitch P, ft	0.349	0.386
Pitch/diameter, P/D	0.674	0.745
Expanded area ratio	0.35	0.35
Blade thickness fraction	0.05	0.05

Brooks and Lang[7] have given a procedure for estimating torpedo drag which may be used to obtain an alternate approximation of the resistance. The influence of tail-cone slenderness, nose shape, and parallel middlebody can be evaluated from a simple chart for bodies having a standard degree of directional stability. Geometric similarity to a standard shape is also implied but, for comparison purposes, this method will be applied although the model shape does not conform to the standard nor is its directional stability known. The tail-cone slenderness l_t^*/d = (length of run aft of the maximum section) divided by d_{eq} is 1.63. The models have virtually no parallel middlebody and the nose shape correction factor is negligibly small, according to the procedure, although it is noted that "for very short bodies, the form drag may be influenced by the nose shape."[7] The model, of course, has an asymmetrical nose which is only roughly fair, which may also contribute to increase the drag. The value of $C_{D,\text{est}}$ according to this procedure is 0.066 for $R_n = 1 \times 10^6$, which corresponds (see Fig. 4) to a speed of 3.1 fps. This value is 24% below the measured $C_D = 0.087$.

Accurate estimation of the resistance of this particular deep submergence vehicle model probably could not be done in a rational way without model testing. It is felt that the "nonstandard" features of this design are not unusual and a similar situation exists for many other vehicle shapes.

The extrapolation of the measured model drag to full scale will be discussed in the section on powering prediction.

Propeller Open-Water Tests

Two three-bladed propeller model shaving different pitch-to-diameter ratios were fabricated of brass so that the influence of pitch ratio on the propeller-hull interaction factors could be assessed. An often-used assumption is that the propeller-hull interaction effects can be derived for a given hull by the use of a "stock" propeller having the same diameter and other characteristics as similar as possible to the anticipated final design of propeller. For some cases, the interaction effects are sensitive to the details of propeller characteristics, and even pitch distribution may have an important influence,[8] so the present tests were planned to give an indication of the adequacy of the use of stock propellers for these hull forms.

The propellers (designated A and B) have the geometrical characteristics shown in Table 1. The blade outline, section shapes, etc., are similar to the Troost methodical series B3.35-type[9] except the present models incorporate zero rake. The model size corresponds to 2.333 ft for the prototype propeller diameter. The pitch is uniform for all radii for these propellers.

Measurements of propeller thrust, torque, rpm, and speed of advance were made for both of the model propellers. In this case, the propeller was mounted on a shaft (see Fig. 6 below) which was supported by a long, slender sting projecting about 3 ft forward of the nose of a propeller-test boat. In this way the propeller was operating in essentially undisturbed, or open-water flow conditions. A nose fairing was mounted on the shaft ahead of the forward face of the propeller hub to obtain smooth flow to the propeller blades. Depth of immersion of the shaft centerline was approximately one propeller diameter.

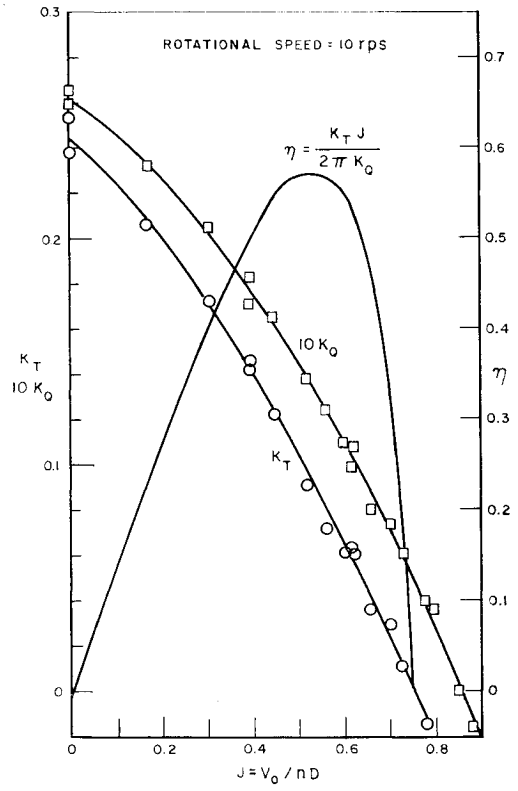

Fig. 7 Open-water test results propeller $A(P/D = 0.674)$.

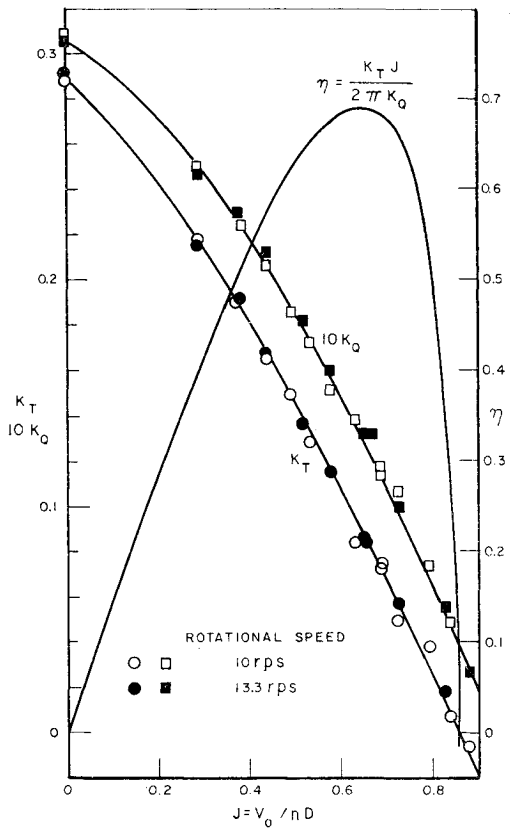

Fig. 8 Open-water test results propeller $B(P/D = 0.745)$.

The test results are presented in Figs. 7 and 8 where the propeller characteristic curves, viz., the thrust and torque coefficients and the efficiency, are plotted on a base of advance coefficient. These terms are defined as follows:

$$\text{thrust coefficient} = K_T = \text{thrust}/\rho n^2 D^4$$
$$\text{torque coefficient} = K_Q = \text{torque}/\rho n^2 D^5$$
$$\text{advance coefficient} = J = V_0/nD \qquad (2)$$
$$\text{efficiency} = \eta = (\text{thrust} \times V_0)/(2\pi n \times \text{torque}) = K_T J/2\pi K_Q$$

where n is propeller rps and V_0 is the open-water propeller advance speed in fps.

Tests were carried out by making runs at various propeller boat advance speeds with approximately the same rotational speed used for each run. This procedure, which is commonly employed in propeller test work, results in similar Reynolds numbers for various advance coefficients since the relative velocity of the blade sections is influenced much more by rotational speed than by advance speed. Tests of both of the propellers were carried out at approximately 10 rps, which is in the range of the rps which were used in the vehicle propulsion tests. In addition, tests of Propeller B were conducted at approximately 13.3 rps. It will be seen from the results (see Fig 8) that the influence of rotational speed on the characteristic curves is not important in this range.

Propulsion Tests

The self-propelled model tests were conducted according to the so-called British or, overload and underload, method. Measurements of propeller thrust and torque and model towing force, measured between the model and the towing strut, were made at various propeller rpm for certain fixed model speeds. All of these data are then used in conjunction with the model propeller open-water test data and the model resistance data to obtain the propeller-hull interaction effects which describe, in essence, the effect of the vehicle's flowfield in causing the water speed to be different from the vehicle's speed (wake fraction) and the effect of the propeller's flowfield in causing an augment to the vehicle's resistance (thrust deduction fraction). This information can then be used, together with propulsion motor characteristics, to prepare a suitable final design for the prototype propeller.

The box which contains the propeller motor and thrust and torque dynamometer was pressurized with nitrogen gas to assure that the motor and dynamometer transducers stayed dry. The pressure regulator was adjusted so that a small bubble of gas was emitted from the shaft bearing occasionally as the shaft rotates. With this system, the shaft ran freely in the bearing and the friction associated with a shaft seal was avoided. The gas flow rate was quite small and did not affect the measured forces. The propeller dynamometer was calibrated, in situ, with the shaft rotating at a slow rpm. Thrust forces were applied through a yoke and bridle, the yoke being secured to the shaft through a ball-bearing. The torque was calibrated using a friction-brake apparatus. A check of the torque vs rpm of the shaft, in water, with a dummy spinner whose weight is the same as the propeller's, indicated that the bearing torque tare is negligible.

Tests were carried out with both afterbody models using both propellers. The results obtained from these tests are presented in Figs. 9 and 10. The actual data points are shown for one of the tests in each of these figures to illustrate data quality, but are omitted for the other tests to avoid unduly cluttering the chart. Although, in principle, a nondimensional presentation of data is desirable, the absolute force levels presented for these tests are convenient for this case, especially since test results for both $V = 0$ and rpm $= 0$ are given. The utilization of the data will be described in the section on power predictions.

Wake Survey Tests

Measurements of the water speed at various points in the plane of the propeller (with the propeller removed) for the

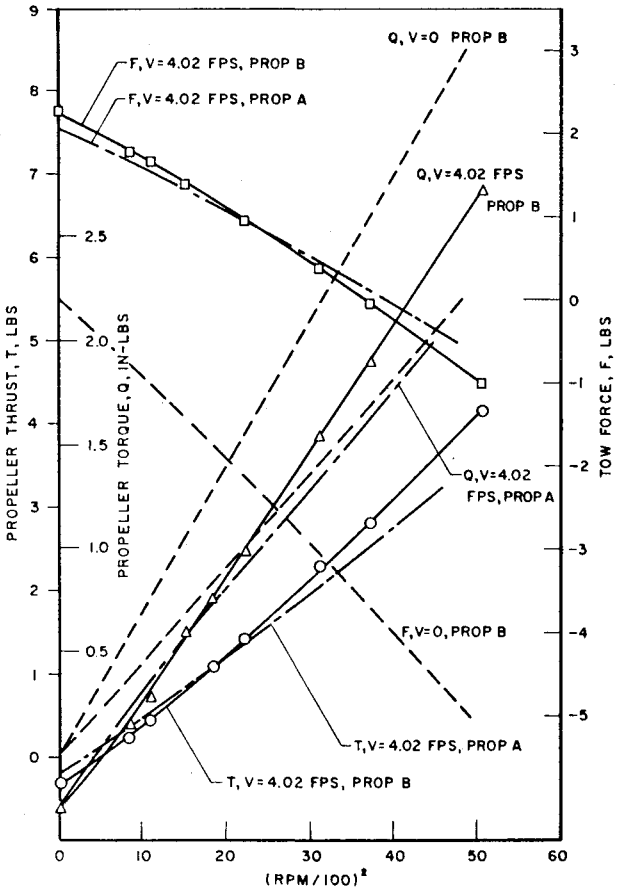

Fig. 9 Propulsion tests results long afterbody model.

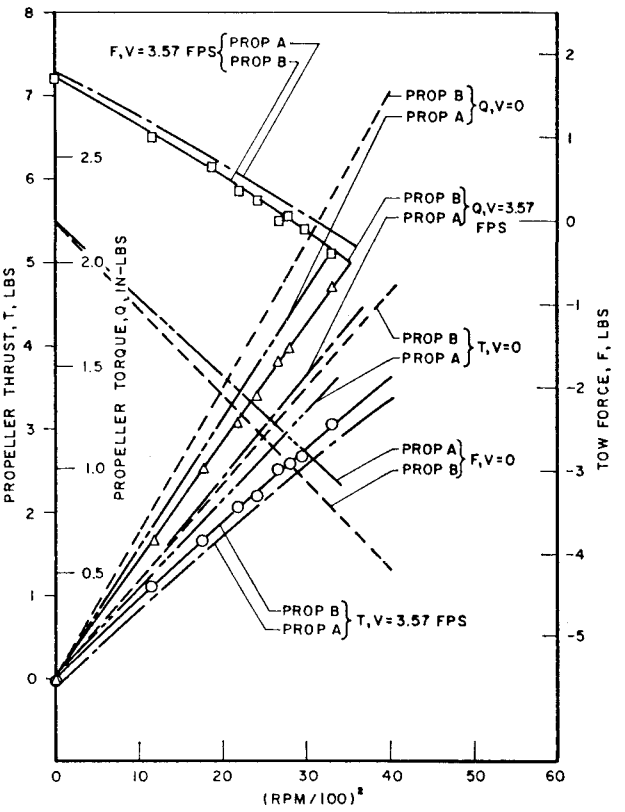

Fig. 10 Propulsion test results short afterbody model.

long afterbody model only, were made using a Prandtl-type Pitot tube. The total pressure and the static pressure were transmitted to opposed chambers of a pressure transducer through water-filled tubing and the difference transduced into an electronic signal. This signal was calibrated vs speed by towing the Pitot tube, alone, through the tank at various speeds. The pressure difference signal is proportional to the square of the velocity as long as the angle of the Pitot tube axis with respect to the flow is less than 17°.[10] The direction of flow, however, cannot be determined with this instrument.

Velocities were determined for various angular locations and for three different radii from the shaft axis corresponding to 0.9, 0.7, and 0.5 of the propeller tip radius. Most of the measurements were made for locations on the starboard side of the vertical centerplane. The model yaw was carefully adjusted to obtain symmetry of the flow. Test results are shown in Fig. 11 where the ratio of flow velocity at a point in the propeller plane to the vehicle speed (4.02 fps for these tests) is plotted on a base of angular orientation of the point for the three radius values. For those points for which the velocity indicated is zero, the measured pressure difference is zero. This may mean that the fluid velocity in way of these areas is in the same direction as the vehicle velocity although the Pitot tube is not able to detect this and it does not seem likely that following flow would be of significant magnitude. Actually, the zero pressure difference could indicate that the angle of the flow relative to the Pitot tube was very large, of the order of 50°, but this is again unlikely since the largest buttock angle on the model, which determines the flow direction at the model's surface, is only around 35° at the trailing edge of the model, and the flow at a distance from the model surface would be expected to be more nearly in a fore-and-aft direction.

The measurements indicate that the average wake speed is indeed very low over a large portion of the propeller plane, at least in the absence of the propeller. The average values of the wake speed as fractions of the vehicle speed at 0.9, 0.7, and 0.5 of the tip radius are 0.54, 0.34, and 0.20, respectively. These averages are based on assuming that the wake velocity does not become negative but is merely zero for certain parts of the propeller plane. The volumetric mean value of the wake speed over the whole propeller plane found by integrating to get the volume under the wake speed "surface" over the disk of the propeller, then dividing by the disk area, is 0.366 times the vehicle speed. Correlation of the Pitot-tube measured wake with results of the self-propelled model tests and their use in the design of the wake-adapted propeller will be discussed below.

III. Powering Predictions

The data presented in the previous sections will be used to evaluate some of the features of propeller-hull interaction, required power and rpm, and propeller selection for vehicles similar to the models tested. Additional plausible approximations are also introduced to assess the qualities of twin-screw vehicles of similar shape and with similar resistance characteristics. The self-propelled model tests data are to be analyzed according to the Froude method where the power required to turn the propeller is

$$P_D = 2\pi Qn/550 = (R_s V_s/550) \times (1 - w_T)/(1 - t) \times (Q/Q_0) \times (2\pi Q_0 n/TV_A) \quad (3)$$

where the following list of definitions applies:

P_D = delivered power at propeller
Q = propeller torque, ft-lb
n = propeller rps
R_s = ship resistance, lb
V_s = ship speed, fps
w_T = Taylor wake fraction determined from thrust identity

Table 2 Full-size propulsive coefficient factors

Load factor 1 $+x$ = 1.0								
Model	t	J_T	w_T	η_H	η_R	η_0 (with test prop.)	η_D	c_D/η_D
Long afterbody, prop. A	0.315	0.286	0.644	1.92	1.12	0.389	0.837	0.0898
prop. B	0.359	0.366	0.550	1.43	1.07	0.493	0.754	0.0998
Short afterbody, prop. A	0.362	0.110	0.859	4.52	1.19	0.154	0.829	0.113
prop. B	0.336	0.187	0.776	2.96	1.14	0.268	0.904	0.1036

t = thrust deduction fraction
Q_0 = propeller torque for "open-water" conditions
T = propeller thrust, = $R_s/(1 - t)$, lb
V_A = propeller speed of advance = $V_s(1 - w_T)$, fps
and
$R_sV_s/550 = P_E$ = effective hp
$(1 - t)/(1 - w_T) = \eta_H$ = hull efficiency
$Q_0/Q = \eta_R$ = relative rotative efficiency
$TV_A/2\pi Q_0 n = \eta_0$ = open-water propeller efficiency
In the analysis given previously, the wake fraction is derived using the so-called "thrust identity" method and the relative rotative efficiency is introduced because the torque absorbed by the propeller behind the model (or ship) may be different from that for the open-water test for equal thrust and rpm, due to differences in radial and peripheral distribution of inflow velocities and other causes. The propulsive coefficient η_D is defined as the ratio of P_E to P_D, and is equal to the product $\eta_H \times \eta_R \times \eta_0$.

The thrust deduction coefficient can be derived from the model test data as

$$t = 1 - (\text{model resistance} - \text{tow force})/\text{model propeller thrust} \quad (4)$$

The model resistance is obtained by extrapolating the specific resistance vs speed tests conducted without a propeller attached. The tow force correction is applied so that the propeller loading corresponds to proper full-scale conditions where the specific resistance may be lower due to lower specific frictional resistance at higher Reynolds number, or it may be higher due to surface roughness effects or added appendages or hull protuberances. The thrust is obtained by entering the self-propelled model test data curves (Figs. 9 and 10) with the calculated value for tow force (positive if specific resistance is lower for the operating point than for the model test conditions) and reading the propeller thrust at the corresponding propeller rpm.

The full-scale specific resistance C_{D_s} will be expressed in terms of a basic value C'_{D_s} multiplied by a load factor $(1 + x)$. The basic value will be determined by extrapolating the data of Fig. 5 to the full-size Reynolds number with the assumption that the specific residuary resistance is a constant. The Schoenherr friction formulation is used[3] and the extrapolation is made to the full-size (scale ratio of 4.5) vehicle operating in sea water at 59°F.†

The wake fraction is derived by using the measured thrust and rpm to calculate a value of K_T, then entering the open-water propeller characteristic curves with this value and reading out the advance coefficient J_T. From this and the known propeller rpm and diameter, the speed of advance V_A is obtained and thence the wake fraction.

† Water temperature of 59°F is a standard vessel condition for most surface-ship powering predictions. It may not be suitable for many deep-submergence vehicles but its effect on the powering prediction will usually be negligible.

The relative rotative efficiency is obtained by deriving the torque for open water from the K_{Q0} value corresponding to the advance coefficient derived on the thrust identity basis and dividing by the torque for the behind ship condition from the self-propelled model test data curves.

The open-water propeller efficiency can be read from the open-water propeller characteristic curves for the propeller used in the tests. Alternatively, the derived propulsion factors can be used to select a more suitable propeller, whose characteristics and open-water efficiency can be arrived at using published information (e.g., Troost's propeller series[9] or calculation). This approach leads to a slightly better estimate of the achievable propulsive coefficient.

Effect of Hull Form and Propeller Pitch

For the full-size vehicles at 3-knots speed, the extrapolated drag coefficients are $C'_{D_s} = 0.0752$ for the long afterbody model and $C'_{D_s} = 0.0935$ for the short afterbody model. The full-size Reynolds numbers are approximately 6 times as high as those for the data used in establishing the model specific resistance. These values have been used with the load factor $1 + x$ = unity, to derive the propulsive performance from the data of Figs. 7–10. Results of the analysis of the data for the 4 tests (two model hulls, two propellers) are presented in Table 2.

It is interesting to note that the ratio of drag coefficient to propulsive coefficient, which is a measure of the power required to drive the vessel, that is, $P_D = (1/550)\cdot(\rho/2) \times A_M V^3 C_D/\eta_D$, is roughly the same for both the long and the short afterbody hull forms. In fact, if the results with the low pitch ratio propeller A are omitted from comparison, the power requirements are within 4% of one another.

The use of the propeller as a wake meter may be accompanied by errors due to lack of precision when the wake speed is very low. This corresponds to low values of advance co-

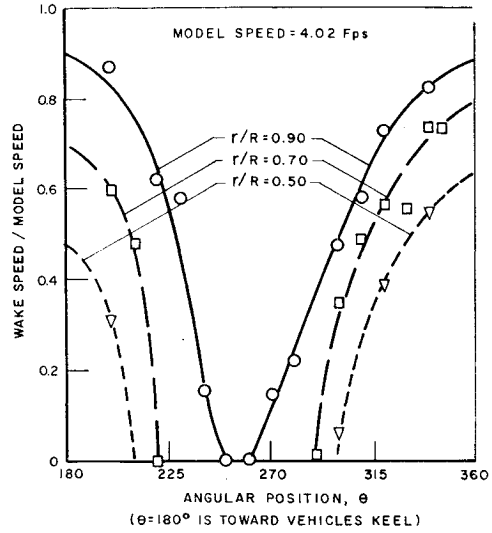

Fig. 11 Wake survey test results long afterbody model.

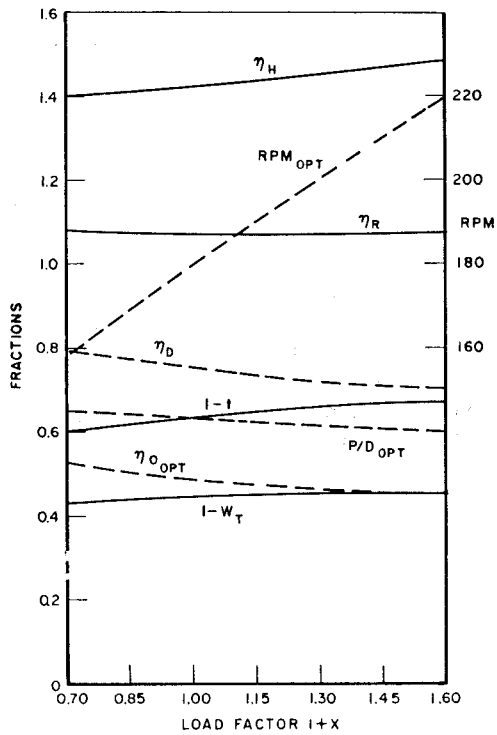

Fig. 12 Effect of load factor on propulsive qualities long afterbody model.

efficient, J_T for thrust identity condition, for which the open-water characteristic curves are subject to scatter of the data,[11] especially if the test Reynolds number is low. The derived values of w_T and η_R are thus questionable although the values for t and η_D, which do not depend on the open-water propeller test results, are not subject to the same degree of criticism. The reliability of the data obtained with propeller A is not considered to be as satisfactory as that for the higher pitch propeller, partly because fewer data points were recorded for the tests with propeller A. This aspect of the results presented in Table 2 is felt to be significant for planning of future tests for these types of vehicles, having extremely high wake fractions. To minimize this problem in future test work, it is suggested that the test propellers have wider blades than are anticipated or required for the full-scale vehicle in order to increase the section Reynolds number and, hence, stabilize the flow about the propeller blades and reduce scale effects, data scatter, etc.

The results of the tests with the long afterbody model fitted with the higher pitch propeller B are considered to be reliable and will be used for further analysis of the influence of load factor and propeller diameter on the powering performance.

Effect of Load Factor

The influence of the load factor on the propeller-hull interaction factors has been determined from the tests of the long afterbody hull in conjunction with the high pitch ratio propeller B. Values of $(1 - t)$, $(1 - w_T)$, η_H, and η_R for a wide range of $(1 + x)$, from 0.7 to 1.6 are given in Fig. 12 where it is seen that these quantities are relatively insensitive to the load factor over a wide range. An assumption which is intrinsic in the use of the overload and underload propulsive test results to derive these quantities is that the propeller loading is the only variable which affects the interaction. Of course, for the full-size load factor to vary as drastically as shown in Fig. 12 practically implies either enormous scale effect or some modification of the hull configuration (e.g., roughness, appendages, etc.) which very likely produce independent effects on the interaction factors. The magnitude of these effects could not be estimated unless the specific hull modifications were stated, and it is likely that more extensive tests would be required in order to make meaningfully accurate estimates in many cases.

Propeller characteristics suitable for the data given in Fig. 12 have been selected from the Troost methodical propeller series,[9] using the B_u vs δ charts for three-bladed propellers having 0.35 developed area ratio. The best efficiency, optimum P/D, optimum rpm and resulting propulsive coefficient are presented in Fig. 12. A separate investigation indicated that this type of propeller (B3.35) has superior performance relative to propellers with greater or fewer blades and to three-bladed propellers with higher developed area ratio. For this type of vehicle, where cavitation liability is not a problem, the propeller area ratio is determined by considerations of efficiency and structural integrity. If the propeller is made of a low weight plastic material, such as nylon, the 0.35 area ratio is about as low as is practicable for this vehicle, to avoid excessively thick sections.

The flat character of the optimum pitch ratio (and other curves in Fig. 12) vs $(1 + x)$ is significant for design and operation of a vehicle similar to this model. If, for instance, the propeller fitted to the vessel is selected to suit a load factor $(1 + x)$ of unity, and the vehicle is operated with extraneous externally mounted gear, the propeller will still be quite suitable. The specific operating condition at off-design propeller loading depends slightly on the propulsion motor's torque vs rpm capability characteristics. For $(1 + x) = 1.6$, the propeller suitable for unity load factor would operate at 166 rpm and absorb only 85% of rated power for a motor whose maximum torque is proportional to the rpm, while for a motor (and speed control system) which can provide constant power, the rpm would be 175.5. The vehicle speed would be 2.51 knots in the latter case and 2.38 knots in the former, compared to a design speed of 3 knots with $(1 + x) = 1.0$.

Effect of Propeller Diameter

The effect of propeller diameter on the best efficiency, pitch ratio and rpm can be derived making use of the nominal wake data presented in Fig. 11 and discussed previously. The average nominal wake speed, determined as the volumetric mean speed for various propeller diameters, is corrected to an effective wake speed by multiplying by the ratio of $(1 - w_T)$ from the self-propulsion tests to the average wake speed as a fraction of the vehicle speed from the Pitot-tube surveys for the test

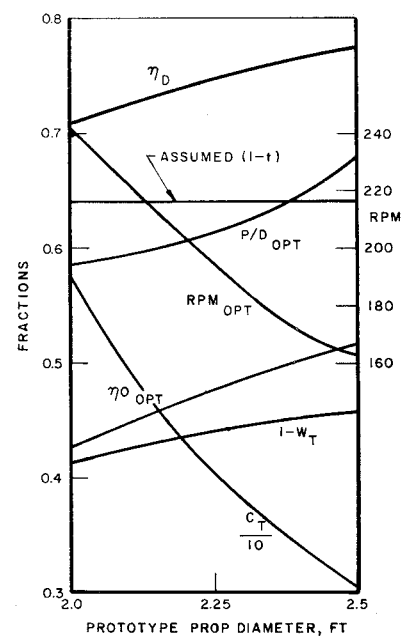

Fig. 13 Effect of propeller diameter on propulsive qualities long afterbody model unity load factor.

propeller diameter, viz., 0.45/0.366 = 1.23, for a unity load factor. This effective wake speed is shown plotted against propeller diameter in Fig. 13 for a range of prototype-size diameters of 2.0 to 2.5 ft.

Experiments which would reveal the effect of propeller diameter on thrust deduction fraction were not conducted for this model. Results of tests with single-screw surface ship models, reviewed by Harvald,[12] do not reveal consistent variations in the thrust deduction fraction with propeller diameter but do indicate, in general, that the effect is small. For the purposes of this analysis, the thrust deduction fraction will be taken to be constant so that $1 - t = 0.641$, as illustrated in Fig. 13.

Again, the Troost methodical series B3.35 propeller data have been utilized to select the optimum rpm and P/D and the corresponding open-water efficiency determined. Assuming relative rotative efficiency is independent of propeller diameter, the propulsive coefficients have been computed. These results are also presented in Fig. 13. A 5% change in propeller diameter from the standard 28-in-size results in approximately 2% change in η_D and 7–10% change in optimum rpm, the larger propeller size having better efficiency and lower rpm, as is to be anticipated.

Alternate Propulsors

Accurate prediction of the performance of a vehicle similar to the present models but having a different type of main propulsion device is somewhat tenuous in the absence of effective means for estimating the propeller-hull interaction effects. For instance, if twin screws driven by right angle drives mounted near amidships are employed, one might assume that the propeller and hull performances are independent of one another. Such an approximation is rather crude but may be indicative of trends for preliminary estimates. The premise of zero-wake fraction for screws located abeam of the vehicle implies that the positive wake due to the friction belt is offset by the negative wake (velocity augment) due to potential flow pressure distribution.

The performance of screw propellers having limited diameters is known to be improved by fitting flow accelerating nozzles ("Kort" nozzles). The optimum performance of this type of propulsor, as a function of propeller loading, has been given by van Manen and Oosterveld,[13] based on extensive experimental results. These results are shown in Fig. 14 where the best achievable open-water efficiency of some marine propulsion devices is shown as a function of $C_T = 2T/\rho V_A^2 A_0$ where A_0 is the area swept out by the tips of the propulsor. This figure is an adaptation of one given by Hoyt and Taggart[14] in 1961 incorporating recently published test data.

The data for propellers in accelerating nozzles indicate the possibility of improved efficiency even for propeller loadings as low as $C_T = 1.0$. It should be noted, however, that the nozzle outside diameter is substantially greater than the propeller diameter and an unshrouded propeller which would fit in the same space would benefit from the increased diameter which it would have.

Table 3 gives the loading coefficient C_T and the estimated propulsive coefficient η_D for the long afterbody hull with

Table 3 Loading and propulsive coefficient

Propeller type	Size	C_T	$\eta_D (\approx \eta_0$, except for stern-mounted prop.)
Single, stern-mounted	28-in. diam	3.93	0.757
Twin, wing-mounted nozzle	8-in. diam	2.88	0.58
	10-in. diam	1.85	0.62
	12-in. diam	1.28	0.67

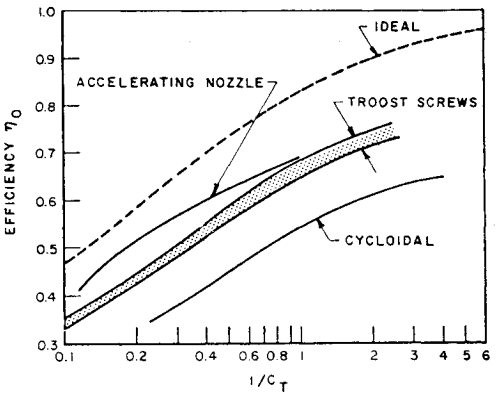

Fig. 14 Optimum open-water efficiency of various types of propellers.

$1 + x$ = unity, having two wing-mounted propellers with varying diameters. The values for C_T and η_D for the stern-mounted screw propeller, discussed previously, are also presented.

It should be emphasized that the performance for the wing-screws have been estimated neglecting propeller-hull interaction and without assessing an appendage-drag penalty for right-angle drive systems, struts, etc. Tests are required to determine whether the assumptions are adequate. A further point which can be drawn from Table 3 and Fig. 14 is that the stern-mounted screw may benefit in performance by incorporating an accelerating nozzle. Again, tests would be required to evaluate how much gain would be achieved since the shrouded propeller would have a smaller diameter and the propeller-hull interaction would be affected.

The use of two wing-mounted screws for main propulsion may be chosen to obtain the maneuverability which would result with rotatable drive system. Another propulsion device which also affords high maneuverability is the cycloidal propeller. Optimum efficiency as a function of C_T for these devices is also shown in Fig. 14 based on data of tests by Ficken.[15] This performance curve is substantially below the curves presented by Hoyt and Taggart[14] for Voith-Schneider and Kirsten-Boeing propellers, which were clearly overly optimistic. No attempt will be made to estimate the propulsive performance of the vehicle fitted with cycloidal propellers because the hull form would need modification to accommodate them and because, in the absence of test data, propeller-hull interaction effects for this device cannot be reasonably estimated.

Other types of propulsors for this vehicle might be contemplated, such as contra-rotating propellers, twin-screws mounted on the "wing tips" of the tail, or twin screws at the tail with overlapping tips, where the blade rotation is either synchronized, or the propellers are staggered in the fore-and-aft direction (to avoid blade clashing). The latter configuration has been studied by Pien[16] for surface ships. Comparisons of the hydrodynamic performance of such arrangements would entail many assumptions which would be tantamount to guessing; consequently, it will merely be remarked that the efficiencies of any of these arrangements could be expected to be fairly good.

A complete design-analysis of different propulsion systems requires, of course, consideration of the propulsion motors, controls, reduction gears, transmission systems effect on other hull arrangements, maneuverability, etc. These are beyond the scope of the present paper.

IV. Full-Scale Trials

Propulsive performance evaluation trials for deep-submergence vehicles should provide valuable engineering information for application to future designs as well as to give

confidence in future operational performance. Such trials can, and should, follow along the lines of trials of larger submarines and surface vessels. The propeller shaft or shafts should be instrumented so that propeller thrust, torque and rpm can be determined and a means for determining the vehicle's speed through the water provided.

Analysis of the results of such trials can follow, at least in part, the analysis procedures used for model tests. Wake fraction may be determined from measured thrust and rpm, together with propeller open-water characteristic curves (usually model scale data). The measured thrust is the ratio of full-size resistance divided by $(1 - t)$. The thrust deduction fraction t is liable to scale effect just as the resistance is; consequently, an independent evaluation of resistance is desirable.

The method of free-deceleration offers a possible way for deriving the full-scale resistance by tests which are not unduly difficult or time-consuming. For a submerged vehicle in static equilibrium, the resistance of the vehicle moving without power is given by

$$\text{resistance} = \rho\nabla(dV/dt) \tag{5}$$

where ∇ is the virtual volume and dV/dt is the deceleration. The virtual volume of the vehicle is the volume displaced by the external skin plus the volume of entrained water. The entrained water can be estimated from potential flow theory for accelerating motion of bodies, values for ellipsoids being given by Lamb.[17] The frictional wake also contributes to the entrained water but a quantitative estimate is not easily made. Perhaps the best procedure which can be suggested is to obtain the entrained water correction factor from specially conducted scale model tests. The correction will be small for most vehicle forms.

Direct measurement of the deceleration is very difficult because of the possible large influence of small trim angles on the longitudinal acceleration sensed by a transducer fixed to the vehicle. A gyro-stabilized platform could alleviate this problem, but the expense of installation is likely to be high. If the resistance can be expressed in the usual form

$$\text{resistance} = C_D(\rho/2)A_M V^2 \tag{6}$$

Equation (5) can be set equal to Eq. (6) and a first integral obtained, viz:

$$t - t_0 = (2\nabla/C_D A_M)(1/V - 1/V_0)$$

where t_0 and V_0 are the initial time and speed. Thus, C_D can be determined from the slope of a $1/V$ vs t plot. Water speed may be determined from a Pitot-tube mounted so that it is not affected by the vehicle's flowfield, or some equivalent device.

To minimize the propeller's effect on this determination of the hull resistance, it is suggested that the motor speed be adjusted to achieve zero thrust on the shaft, perhaps through a control system using thrust-meter feedback. Since no flow is being induced by the propeller in this condition the thrust deduction fraction should be zero. The vehicle should be kept in level trim during the trial. One of the recommendations pursuant to trials of the airship USS LOS ANGELES in 1927[18] was that the pilot keep level trim by observing a distant object rather than by using the indications of an inclinometer or his senses because of the influence of longitudinal deceleration.

The accuracy of such tests depends on how faithfully the actual test conditions conform to the desired steady-state conditions and on the accuracy of the apparatus and of the entrained water factor. In 1931, Thompson and Kirschbaum[19] indicated that results with airships were probably accurate to within $\pm 8\%$. It is felt that better accuracy can be achieved now because of better instrumentation, control of propeller influence and model test evaluation of the entrained water effect. An interesting summary of many tests conducted to determine the added mass for various body shapes has been given by Smith.[20]

The conduct of tests of this kind would produce useful information on scale effect on the unusual hull forms typical of many deep-submergence vehicles and would also provide data on appendage drag of externally mounted equipment, which cannot be successfully evaluated in small model tests because of the danger of large scale effects.

V. Summary

1) Results of comprehensive model powering tests conducted with two alternate hull configurations for a deep-submergence vehicle having a single, stern-mounted propeller are presented and discussed. The use of the data in predicting the full-size power requirements for various operating conditions is outlined. A comparison of the resistance data with two published methods for estimating the drag of bodies of revolution indicates that an accurate estimate of this quantity could probably not be obtained without model testing. No comparison of propulsion factors is presented because, to the author's knowledge, suitable comparative data are not available in the published literature. 2) Analysis of the powering data for both hulls, fitted with each of two alternate propellers, all for a given full-size loading condition, demonstrates that the shorter afterbody hull, which has 20% higher drag, requires only 4% more power to drive. Tests results with one of the propellers (Prop. A) are considered questionable because of possible lack of data precision for low advance speed of the propeller. 3) The infiuence of propeller loading on the propeller-hull interaction effects and on the power requirements has been determined from the tests of the long afterbody hull in conjunction with propeller B. Propeller loading variation might be associated with unaccounted-for scale-effect, hull roughness, extraneous appendages, etc. The propulsive factors are found to be relativley independent of the loading. 4) Results of wake survey tests in the plane of the propeller, together with additional reasonable approximations, have been used to evaluate the influence of propeller diameter on the propulsive performance. A 5% change in propeller diameter produces a 2% change in the over-all propulsive efficiency. 5) A brief discussion of alternate propulsion arrangements is presented. It appears that twin screws, mounted abeam of the hull, would not have propulsive efficiency as high as the single stern-mounted propeller, but the penalty need not be great. 6) Full-scale powering trials, wherein vehicle speed and propeller thrust, torque, and rpm are measured, are recommended to provide valuable engineering information for application to future designs and to assure satisfactory vehicle operation. Free-deceleration tests to evaluate the full-scale resistance of these vehicles are advocated.

VI. References

[1] Wenk, E., "Submarines to Advance Study and Effective Use of the Sea," *Experimental Mechanics*, Vol. 8, No. 8, Aug. 1968, pp. 337–348.

[2] Hoerner, S. F., *Fluid Dynamic Drag*, published by the author, Midland Park, N. J., 1958.

[3] Todd, F. H., "Tables of Coefficients for ATTC Model-Ship Correlation and Kinematic Viscosity and Density of Fresh and Salt Water," T&R Bulletin 1–25, 1964, Society of Naval Architects and Marine Engineers.

[4] Wigley, W. C. S., "Water Forces on Submerged Bodies in Motion." *Transactions of Institution of Naval Architects*, Vol. 95, 1953, pp. 268–279.

[5] Roshko, A., "Experiments on the Flow Past a Circular Cylinder at Very High Reynolds Number," *Journal of Fluid Mechanics*, Vol. 10, Pt. 3, 1961, pp. 345–356.

[6] Clements, R. E., "The Control of Flow Separation at the Stern of a Ship Model Using Vortex Generators," *Transactions of*

Royal Institution of Naval Architects, Vol. 107, 1965, pp.351–373; also discussion by H. Lackenby.

[7] Brooks, J. D. and Lang, T. G., "Simplified Methods for Estimating Torpedo Drag," NAVORD Rept. 5842, 1958, Naval Ordnance Test Station, China Lake, Calif.; also *Underwater Missile Propulsion*, edited by Greiner, Compass, Arlington, Va., 1967.

[8] Hill, J. G., "The Pitch Distribution of Wake-Adapted Marine Propellers (discussion of paper by L. Troost)," *Transactions of Society of Naval Architects and Marine Engineers*, Vol. 64, 1956, p. 370.

[9] Troost, L., "Open-Water Test Series with Modern Propeller Forms. Part III," *Transactions of North East Coast Institution of Engineers and Shipbuilders*, Vol. 67, 1951, pp. 89–130.

[10] Prandtl, L. and Tietjens, O., *Applied Hydro- and Aeromechanics*, Engineering Societies Monographs, 1934, reprinted by Dover, New York, 1957, pp. 229–231.

[11] Nordstrom, H. F., "Screw Propeller Characteristics," Publ. No. 9, 1948, Swedish State Shipbuilding Experimental Tank, Göteborg.

[12] Harvald, S. A., *Wake of Merchant Ships*, The Danish Technical Press, Copenhagen, 1950.

[13] van Manen, J. D. and Oostervel, M. W. C., "Analysis of Ducted Propeller Design," *Transactions of Society of Naval Architects and Marine Engineers*, Vol. 74, 1966, pp. 522–562.

[14] Hoyt, E. D. and Taggart, R., "Future Trends in Marine Propulsion Systems," RT-4901, Sept. 1961, Robert Taggart Inc., Fairfax, Va.

[15] Ficken, N. L., "Conditions for the Maximum Efficiency Operation of Cycloidal Propellers," Paper presented to the Chesapeake Section, Society of Naval Architects and Marine Engineers, April 6, 1966.

[16] Pien, P. C. and Strom-Tejsen, J., "A Proposed New Stern Arrangement," Rept. 2410, May 1967, Naval Ship Research and Development Center, Washington, D.C.

[17] Lamb, H., *Hydrodynamics*, 6th ed., Dover, New York, 1945, pp. 152–156.

[18] DeFrance, S. J. and Burgess, C. P., "Speed and Deceleration Trials of USS Los Angeles," Rept. 318, 1929, NASA.

[19] Thompson, F. L. and Kirschbaum, H. W., "The Drag Characteristics of Several Airships Determined by Deceleration Tests," Rept. 397, 1931, NASA.

[20] Smith, S. L., "BSRA Resistance Experiments on the Lucy Ashton," *Transactions of Institution of Naval Architects*, Vol. 97, 1955, pp. 525–561.